Computers and Concrete, *Vol. 20, No. 2 (2017) 215-227*
DOI: https://doi.org/10.12989/cac.2017.20.2.215

A model for the restrained shrinkage behavior of concrete bridge deck slabs reinforced with FRP bars

Amir Ghatefar[1a], Ehab ElSalakawy[*2] and Mohamed T. Bassuoni[2b]

[1]*Department of Civil Engineering, Urmia Branch, Islamic Azad University, Urmia, Iran*
[2]*Department of Civil Engineering, University of Manitoba, Winnipeg, Manitoba, Canada*

(Received June 15, 2016, Revised April 11, 2017, Accepted April 14, 2017)

Abstract. A finite element model (FEM) for predicting early-age behavior of reinforced concrete (RC) bridge deck slabs with fiber-reinforced polymer (FRP) bars is presented. In this model, the shrinkage profile of concrete accounted for the effect of surrounding conditions including air flow. The results of the model were verified against the experimental test results, published by the authors. The model was verified for cracking pattern, crack width and spacing, and reinforcement strains in the vicinity of the crack using different types and ratios of longitudinal reinforcement. The FEM was able to predict the experimental results within 6 to 10% error. The verified model was utilized to conduct a parametric study investigating the effect of four key parameters including reinforcement spacing, concrete cover, FRP bar type, and concrete compressive strength on the behavior of FRP-RC bridge deck slabs subjected to restrained shrinkage at early-age. It is concluded that a reinforcement ratio of 0.45% carbon FRP (CFRP) can control the early-age crack width and reinforcement strain in CFRP-RC members subjected to restrained shrinkage. Also, the results indicate that changing the bond-slippage characteristics (sand-coated and ribbed bars) or concrete cover had an insignificant effect on the early-age crack behavior of FRP-RC bridge deck slabs subjected to shrinkage. However, reducing bar spacing and concrete strength resulted in a decrease in crack width and reinforcement strain.

Keywords: GFRP; concrete; deck slabs; early-age cracking; finite element modeling; serviceability

1. Introduction

Since concrete bridge deck slabs usually are much longer in the direction of traffic, they experience transverse early-age cracks due to volumetric instability and restraint conditions (Kwan and Ng 2009). The magnitude of induced tensile stresses depends on both the amount of shrinkage and the degree of restraint (internal and external) (Au *et al*. 2007). These structures are vulnerable to volumetric instability due to changes in daily or seasonal conditions (Zhang *et al*. 2012). Also, in slab-on-girder type bridges, the girders and continuity of slabs restrain the movement of deck slabs due to shrinkage and thermal changes, which induce stresses that result in transverse cracks. There are many other factors affecting early-age cracking in bridge deck slabs such as material properties, construction techniques, and design practices (Hadidi and Saadeghvaziri 2005). In the last two decades, the lower cost of the non-corrodible Glass Fiber Reinforced Polymer (GFRP) bars has made them attractive to the construction industry to mitigate the corrosion problem of conventional steel reinforcement, especially for structures exposed to aggressive environments such as bridge deck slabs and barrier walls (*ISIS Canada* 2007). Compared to steel, FRP bars have a lower modulus of elasticity, therefore, concrete elements reinforced with FRP bars exhibit larger deformation which causes wider cracks under service conditions. The Finite Element Modeling (FEM) provides an effective tool to simulate laboratory conditions with a high degree of accuracy for any complex structural experiment without the constraints of time and cost. This numerical study aims to investigate the effect of key design parameters, namely, concrete strength and cover as well as reinforcement type and spacing, on early-age cracking of FRP-RC bridge deck slabs.

2. Background

2.1 Minimum FRP reinforcement ratio and spacing

The minimum FRP reinforcement ratio for shrinkage and temperature recommended in the current FRP design codes and guidelines such as CSA/S806-12 (CSA 2012) and ACI- 440.1R-15 (ACI Committee 440 2015) has no experimental basis. Most of these codes and guidelines are based on modifying corresponding formulas originally developed for steel bars by taking into account the difference in material properties and behavior between FRP and steel. Based on an experimental study, Koenigsfeld and Myers (2003) concluded that the equation provided in ACI-440.1R-03 (ACI Committee 440 2003) for minimum FRP

∗Corresponding author, Professor and CRC
E-mail: Ehab.El-Salakawy@umanitoba.ca
[a]Assistant Professor
E-mail: Ghatefara@mmm.ca
[b]Associate Professor
E-mail: Mohamed.Bassuoni@umanitoba.ca

ISSN: 1598-8198 (Print), 1598-818X (Online)

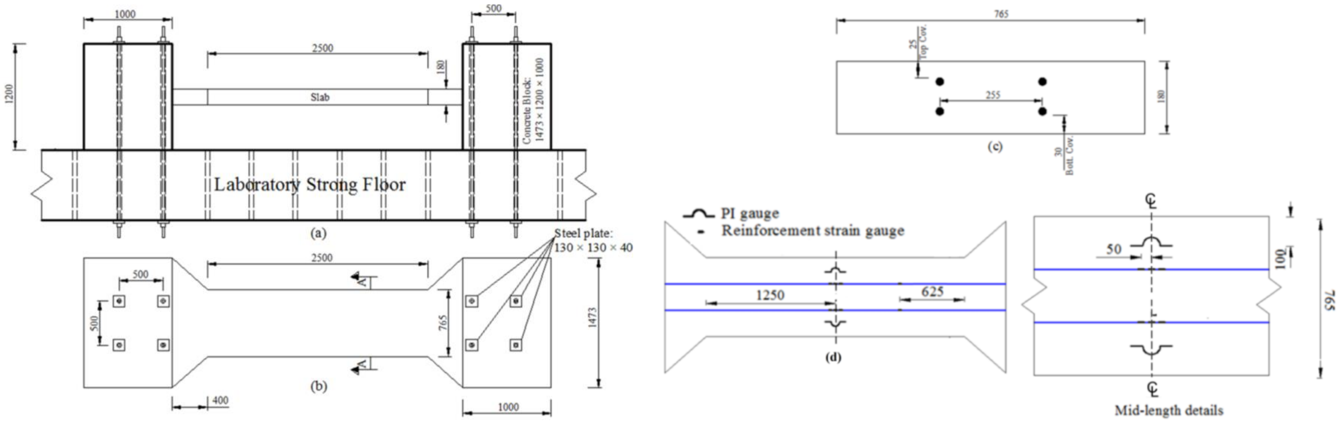
Fig. 1 Deck slab dimensions (all dimensions are in mm): (a) side view, (b) top view, (c) cross-section A-A, and (d) typical instrumentation of a deck slab

reinforcement ratio was overly conservative. Also, they found three times larger crack width for GFRP-RC panels (1830×591×127 mm) than that of counterpart specimens with similar amounts of steel reinforcement when subjected to shrinkage. Recently, Ghatefar *et al*. (2014) concluded that the minimum FRP reinforcement ratio of 0.7% recommended by CHBDC (CSA 2006) can reasonably control the early-age crack width and reinforcement strain under normal laboratory conditions.

2.2 Concrete cover

Concrete cover is essential to protect the reinforcement from aggressive environments and to provide sufficient bond between reinforcing bars and concrete. All design codes for RC structures suggest minimum concrete cover depending on the exposure conditions of the structure. Literature review indicates that concrete cover has an inconsistent influence on crack development in bridge deck slab. Increased cover thickness reduces the tendency of cracking (Ramey *et al*. 1997); however, concrete deck slabs with more than a 75-mm (3 in) thick cover are more susceptible to cracking (Myers 1982).

2.3 Concrete strength

The application of high strength concrete (HSC) has been increased during the past decades. In general, HSC is accompanied by an increase in the cement content and a decrease in the water-to-binder ratio, which results in an increment of hydration temperature and autogenous shrinkage. Therefore, compared to normal strength concrete, RC structures with HSC are more susceptible to early-age cracking. The HSC offers high sectional stiffness (Sooriyaarachchi 2005); thus structures made of HSC experience high tensile stress, and consequently, high cracking potential for the same amount of shrinkage (Hadidi and Saadeghvaziri 2005). However, due to the higher tensile strength of HSC, it also provides higher resistance to shrinkage and thermal cracking. Hence, it is a challenge to maintain a proper balance between concrete strength, shrinkage and other long-term properties (e.g., creep).

2.4 Numerical studies

A limited number of parametric studies using FEM have been carried out on steel-RC bridge deck slabs subjected to shrinkage (Chen *et al*. 2008). According to a FEM study conducted by Hadidi and saadeghvaziri (2005), it was concluded that slab sectional stiffness and girder spacing have a significant impact on early-age cracking patterns and stress histories in steel-RC bridge deck slabs. Also, Minnetyan *et al.* (2011) performed a non-linear FEM (using ABAQUS software) to examine the effect of temperature variation in the external steel girders on early-age cracking in RC bridge deck slabs. They found that cooling the lower flange of the girder, at negative moment regions, during concrete hydration would increase the compressive stresses at the surface of the deck after dissipation of the hydration heat and mitigate tensile stresses due to drying shrinkage.

3. Summary of the experimental program

The experimental study (Ghatefar *et al.* 2014) included four full-size, cast-in-place RC deck slabs measuring 2500-mm long by 765-mm wide by 180-mm thick as shown in Fig. 1. Three slabs were reinforced with different GFRP reinforcement ratios (0.50%, 0.70% and 1.1%), while, one was reinforced with steel (0.7%) as a control. The slab prototypes were constructed in the laboratory and subjected to shrinkage under room-temperature conditions for 112 days. Also, in order to measure the actual shrinkage strain of concrete, one additional un-restrained (free-ends) slab having similar dimensions and materials, was constructed and subjected to the same ambient conditions in the laboratory. The reinforcement configuration of the test specimens was selected based on the empirical design method recommended by Section 16 of the CHBDC (CSA/S6-06). All test prototypes had similar top and bottom clear covers (25 and 30 mm, respectively) and a constant spacing of 255 mm for the longitudinal reinforcement. Normal strength concrete mix incorporating 13% silica fume by mass of binder with a target 28-day compressive strength of 40 MPa was used for all specimens. For the first

24 hours after casting, an extreme scenario that might be encountered in practice with a high tendency for shrinkage was provoked. This was done by building a plastic tent around the test prototypes while electrical heaters were used to maintain the internal concrete temperature at 35℃ without moist curing followed by exposing the slabs to an air flow for 6 days. To measure strains in GFRP bars at the vicinity of the main crack, three strain gauges were installed on each reinforcement bar at both top and bottom layers; one centered at the mid-span, and the other two at 50 mm on each side. Also, the width of cracks was recorded throughout the test using two PI-gauges along the crack length (Fig. 1(d)). The experimental results are summarized in Table 1, while details on this study can be found elsewhere (Ghatefar *et al.* 2014).

4. Finite Element Model (FEM)

This section introduces the fundamental steps to construct the FEM including element types, material models and boundary conditions. A total of four element types were defined in this program to model concrete, steel support plates, end steel bars and main FRP reinforcement.

In the experimental study all slabs were effectively anchored at its ends by 1473×1000×1200 mm concrete blocks. However, in the FEM, those blocks were replaced with 50-mm thick stiff steel end plates to reduce number of elements and solution time. The model generated is shown in Figs. 2(a) and 2(b).One-dimensional (1-D) reinforcement bars were added to the model by first creating two joints to define the start and end points of the reinforcement. The reinforcement layout of the model is shown in Fig. 2(c).

4.1 Concrete

The 3-D eight-node solid brick element (Fig. 3) was used to model the geometry of the slabs (except the corner parts). A brick element is only available to be used for hexahedron-shaped elements. This element is defined by 8 corner nodes with five degrees of freedom (DOFs) at each node; three translations and two rotations in-planes normal to mid-surface of element (Cervenka *et al*. 2012), as well as 12 additional integration points located at the middle of the element side length as shown in Fig. 3(b). The external forces, reactions and displacements can be monitored at corner nodes while stress, strain, temperature, initial stress and strain, body forces and crack attributes can be monitored at the integration points. The brick element is ideal to use whenever it can be since it is generally accurate and can significantly reduce analysis time required by the computer compared to the other element types (Cervenka *et al.* 2005). The geometry of the corner parts were modeled using 3-D four-node tetrahedron solid elements. This element is defined by 4 corner nodes with five DOFs at each node (Cervenka *et al*. 2012), as well as with 6 additional integration points as shown in Fig. 3(c).

Tetrahedron element should be used whenever there is some sort of irregularity in an element, such as an opening on its surface or triangle-shaped elements. The tetrahedron element is more flexible than a brick element but can also result in increased processing time (Cervenka *et al.* 2005).

In this study, the material model "CC3DNonLinCementitious2Variable" was assigned for both concrete brick and tetrahedron elements. Since the concrete properties changes versus time, this material model allows to define time-dependent properties for concrete. Therefore, the equation recommended by ACI 209.2R-08 (ACI Committee 209 2008), Eq. (1), was adopted to estimate the strength development of concrete as a function of time, using concrete compressive strength at age 28 days (t (day) and $f'_{c,t}$, $f'_{c,28}$ (MPa)).

$$f'_{c,t} = [\frac{t}{4+0.85t}]\, f'_{c,28} \tag{1}$$

The "CC3DNonLinCementitious2Variable" material model is able to account for the nonlinearity of concrete and provides smeared cracking information in the three main perpendicular directions. The concrete fracture is modelled by a smeared crack model based on Rankine tensile criterion (Cervenka *et al.* 2012).

Table 1 Summary of experimental results at 112 days after casting

Slab*	w (mm) & ε (με)	Exp.
SG1	ε	2480
	w	0.64
SG2	ε	1520
	w	0.33
SG3	ε	1000
	w	0.24
SS	ε	410
	w	0.19

* w (*mm*) & ε ($\mu\varepsilon$): the average crack width and strain in reinforcement at crack location, respectively. Exp.: the final experimental results

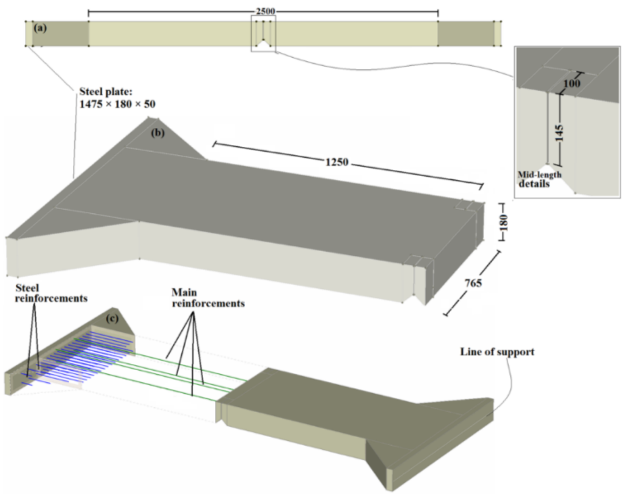

Fig. 2 Model geometry: (a) side view, (b) 3D view of the analytical model based on the experimental test specimens, and (c) locations of the reinforcing bars (all dimensions are in mm)

The concrete plasticity model is based on the Menetrey-William failure surface equation (Cervenka *et al.* 2012).

The Menetrey-Willam failure surface adopts the uniaxial compressive test of concrete based on the experimental work of Van Mier (Cervenka *et al.* 2012), where in the concrete stress-strain relationship, the softening curve is linear (Fig. 4). The elliptical ascending part is given by the following equations

$$\sigma = f_{co}^{'} + (f_c^{'} - f_{co}^{'})\sqrt{1-\left(\frac{\varepsilon_c - (f_c^{'}/E_c)}{\varepsilon_c}\right)^2} \tag{2}$$

$$f_{co}^{'} = 2 f_t^{'} \tag{3}$$

$$w_d = (f_c^{'}/E_c - \varepsilon_c^{\,p})\, L_c \tag{4}$$

where σ is the concrete compressive stress (MPa), E_c is the concrete modulus of elasticity (GPa), f_c' and f_t' are the concrete compressive and tensile strength (MPa), respectively, W_d is the end point of the softening curve (W_d = - 0.0005 mm for normal strength concrete as recommended by the software guidelines), f_{co} is the starting point of the non-linear curve (MPa), ε_c^p is the value of plastic strain at the max compressive strength, on the descending curve, and L_c is the element length scale parameter.

The cracking behavior of concrete was modeled according to the equation developed by Hillerborg (Cervenka *et al.* 2012) (Eq. (5)) as represented in Fig. 4(c).

The width of crack in this equation is calculated based on three factors: the shape of the softening curve, tensile strength and fracture energy. The effect of tension stiffening where cracks cannot fully develop along the section is also considered. Tension stiffening is simulated by specifying a factor that represents the relative limiting value of tensile contribution as a fraction of the tensile capacity of the concrete.

$$\frac{\sigma}{f_t^{'}} = \left(1 + 3067\frac{w}{5.15G_f/f_t^{'}}\right)^3 \exp\left(-6.93\frac{w}{5.15G_f/f_t^{'}}\right) - \left(\frac{w}{5.15G_f/f_t^{'}}(1+3067^3)\right) \tag{5}$$

where w is the crack width (mm), G_f is the concrete fracture energy (MN/m), σ is concrete actual tensile stress (MPa), and f'_t is the concrete tensile strength (MPa). The software generates the concrete properties using the concrete cube strength, f'_{cu} (MPa). Eq. (5) was used to define concrete cube strength from standard cylinder tests. Poisson's ratio was assumed to be 0.2, and the concrete tensile strength, f'_t (MPa), initial modulus of elasticity (E_c) (MPa), and fracture energy (G_f) (MN/m) were calculated based on the following equations used in this software (Cervenka *et al.* 2012)

$$f_{cu}^{'} = 1.15 f_c^{'} \tag{6}$$

$$f_t^{'} = 0.24(f_{cu}^{'})^{2/3} \tag{7}$$

$$E_c = (6000 - 15.5 f_c^{'})\sqrt{f_{cu}^{'}} \tag{8}$$

$$U_L = \frac{1}{2}\left(\int_0^d EI(v_1'')^2\, dx\right) + \frac{1}{2}\left(\int_0^d EA(u_1')^2\, dx\right) \tag{9}$$

4.2 Steel support plates

Lines along the surfaces of the outside edges of the end steel plates were fixed in all directions to simulate fixed end conditions. These plates were modeled using the same brick element but with the 3-D Elastic Isotropic material. The yield strength, modulus of elasticity, and Poisson's ratio were assumed to be 420 MPa, 200 GPa and 0.3, respectively.

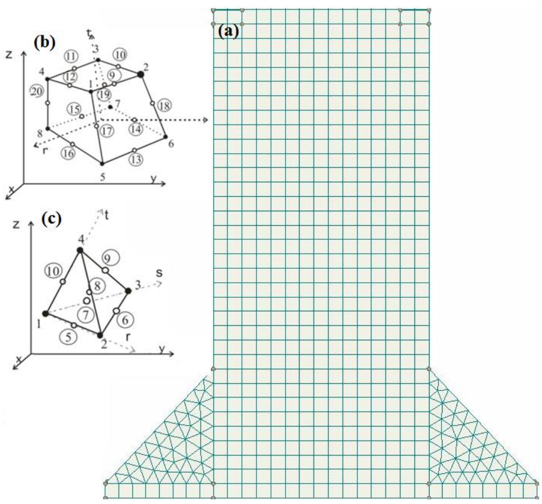

Fig. 3 Different finite element types used**:** (a) Top view of the finite element mesh of the analytical model, (b) brick element, and (c) tetrahedron element

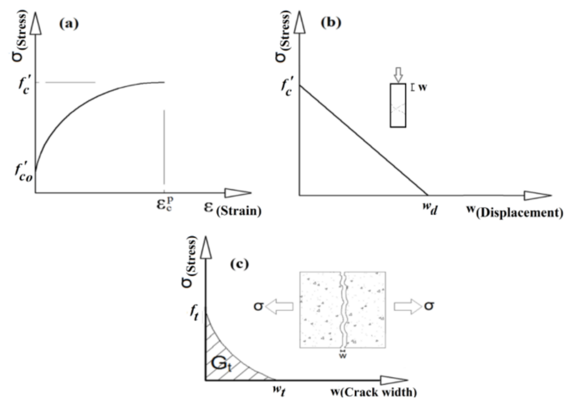

Fig. 4 Van Mier compressive stress-strain relationship of the concrete: (a) non-linear ascending part, (b) linear descending (softening) part, and (c) stress-crack opening according to Hodjik law (reproduced from Cervenka *et al.* 2012)

Table 2 Mechanical properties of GFRP, CFRP and steel bars

Bar type	Bar diameter (mm)	Bar area (mm^2)	Modulus of elasticity (GPa)	Tensile strength (MPa)	Tensile strain (%)
GFRP #4	12.7	127	65	1453	2.23
GFRP #5	15.9	198	62	1450	2.23
GFRP #6	19.1	285	63	1484	2.35
CFRP #4	12.7	127	144	1899	1.32
CFRP #5	15.9	198	140	1648	1.18
Steel 15M	16	200	200	$^*f_y$ = 420	$^*\varepsilon_y$ = 0.21
Steel 25 M	25	500	200	f_y = 420	ε_y = 0.21

$^*f_y$: Steel yield strength, ε_y: Steel yield strain

4.3 Reinforcing bars

Since the bar spacing is an important factor affecting the cracking behavior, the discrete method was selected for modeling reinforcement in the concrete (Mias *et al*. 2013). In this regard, the 1-D "Reinforcement" truss element was used for both FRP and steel reinforcing bars. The basic characteristics of the steel reinforcement were determined using a bi-linear form with yield strength and elastic modulus of 420 MPa and 200 GPa, respectively. The GFRP reinforcement has a linear elastic behavior up to failure.

Table 2 provides the material properties of the reinforcement used in the FEM.

The bond stress-slippage relationship between concrete and reinforcement has a significant effect on the performance of RC structures (Mazaheripour *et al.* 2013). For this model, the stress-slippage relationship was defined using the "Bond for Reinforcement" option. Different bond stress-slippage relationships were used to define the response of bond elements for the steel, GFRP and CFRP bars.

The stress-slippage model recommended by CEB-FIP Model Code (*CEB-FIP* 1990) was used for steel bars (Fig. 5). The interface between reinforcement and surrounding concrete used for different surface pattern of CFRP bars were based on the study by Malvar *et al.* 2003 (Fig. 5). For sand-coated and ribbed-deformed GFRP bars, the interfaces were defined based on the study by Alves *et al.* (2011) and manufacture specifications, respectively (Fig. 5).

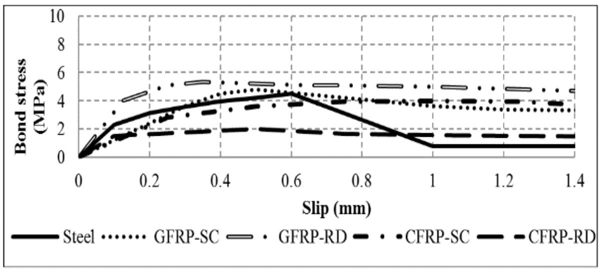

Fig. 5 Bond-slip relationship for different types of reinforcement in concrete at 3 days (f'_c=15 MPa)

4.4 Meshing of the model

In this study, each specimen was meshed into 8545 finite elements with a side length of 50 mm each. Also, each steel end-plate was meshed into 124 elements. Since the program automatically generates embedded finite elements for the reinforcement bars, 1-D entities such as bar does not need to be meshed by the user before the model analysis is started.

4.5 Shrinkage profile

To estimate the shrinkage profile of concrete, ACI 209.2R-08 (ACI Committee 209 2008) recommends different models such as ACI 209 (Eq. 10), Bažant-Baweja B3 (Eq. (11)), GL2000 (Eq. (12)) and CEB-FIP/90 (Eq. (13)) to predict time-dependent shrinkage of concrete.

$$\varepsilon_{sh(t)(ACI209)} = \frac{(t-t_c)}{26e^{\{{}^{V}\!/_{S}1.42\times10^{-2}\}}+(t-t_c)}\gamma_{sh}(-780)\times10^{-6} \quad (10)$$

$$\varepsilon_{sh(t)(B3)} = \tanh\sqrt{\frac{(t-t_c)}{0.85t_c^{-0.08}f_{cm28}^{-0.25}[2\,{}^{v}\!/_{s}]^2}}\,k_{(h)}\times-\varepsilon_{sh(\infty)} \quad (11)$$

$$\varepsilon_{sh(t)(GL2000)} = [\frac{(t-t_c)}{\{t-t_c+0.12(v/s)^2\}}]^{0.5}\beta_{(h)}\times-\varepsilon_{shu} \quad (12)$$

$$\varepsilon_{sh(t)(CEB-MC90)} = [\frac{(t-t_c)}{350[\frac{{}^{v}\!/_{s}}{20}]^2(t-t_c)}]^{0.5}\beta_{RH(h)}\times\varepsilon_{cso} \quad (13)$$

Where γ_{sh} represents the cumulative product of the applicable correction factors for fresh concrete properties and ambient humidity conditions in the ACI 209 model, $\varepsilon_{sh\infty}$, ε_{shu} and ε_{cso} are the notional ultimate shrinkage (*mm/mm*) based on RILEM data bank (RILEM 1998) for

Bazant, GL 2000 and CEB-MC90 equations, respectively. Also, $K_{(h)}$, $\beta_{(h)}$, and $\beta_{RH(h)}$ are the ambient relative humidity factor for Bazant, GL2000 and CEB-MC90 models. Moreover, t and t_c are the concrete age and curing time (day), respectively, and v/s is member's volume-to-surface ratio (mm). In these models the concrete was assumed to be moist cured at least for 1-14 days.

It is well-documented in the literature (Mehta and Monteiro 2014) that ambient environmental conditions in terms of combined temperature and humidity changes affect the amount of concrete shrinkage. However, the effect of temperature on concrete shrinkage is explicit in most of the prediction equations mentioned above. Nevertheless, the CEB-MC90 model incorporates the effect of temperature as well as humidity to predict the shrinkage of concrete versus time. When a constant temperature above 30℃ is applied while the concrete is drying, CEB MC90 recommends Eq. (14) to predict concrete shrinkage.

$$\varepsilon_{sh(t,T)(CEB-MC90)} = [\frac{(t-t_c)}{350[\frac{v/s}{20}]^2 \exp[-0.06(T-20)] + (t-t_c)}]^{0.5} \beta_{RH(h)} [1+(\frac{0.08}{1.03-h})(\frac{T-20}{40})] \beta_{RH(h)} \times \varepsilon_{cso} \quad (14)$$

where: h and T are the ambient relative humidity (%) and temperature (℃), respectively.

In the experimental study, all prototypes were kept inside a plastic tent for 1 day after casting. The profile of shrinkage was accelerated at early-age by increasing the temperature in the tent to 35℃ in the first day followed by exposing the slabs to air flow of 50 km/h for 6 days. Table 3 provides the environmental conditions applied to all specimens.

The CEB-MC90 model was modified to account for the temperature and humidity changes shown in Table 4. The shrinkage strain of concrete ε_{Total} subjected to different environmental conditions was calculated using Eq. (15)

$$\varepsilon_{Total} = \varepsilon_{sh(t)(\text{CEB-MV90})} + \alpha_3 \Delta \mathrm{T} + \mathrm{AF} \quad (15)$$

where α_3 is the concrete coefficient of thermal expansion at age of 3 days (~2.55×10^{-6} per ℃, obtained by ASTM-E831 2013), ΔT is temperature change (℃) between incremental time steps and AF is the effect of air flow on concrete shrinkage ($\mu\varepsilon$).

Table 3 Environmental conditions applied to the slabs versus the time of exposure

Time (Day)	Temperature (℃)	Humidity (%)	Ambient conditions
1	35	85	Slabs subjected to a hot temperature inside a tent
2-8	22	40	Slabs subjected to air flow by fans
8-112	22	65	Slabs subjected to laboratory conditions

Figure 6 shows the concrete free shrinkage versus that predicted by the modified CEB-MC90 model (Eq. (15)). Test results indicate that the advent of air flow at 2 to 7 days led to steady-state shrinkage. Therefore, the rate of shrinkage in this time interval can be calculated by linear interpolation at a rate of 18.2 $\mu\varepsilon$/day. The main part of drying shrinkage caused by air flow (AF) occurred within 2-7 days, therefore the remaining shrinkage predicted by CEB-MC90 was distributed within 8-112 days using the model's time function (Eq. (16)). Figure 6 indicates that the modified CEB-MC90 model could reasonably predict the concrete total shrinkage based on the applied environmental conditions.

$$[\frac{(t-t_c)}{350[\frac{(v/s)}{50}]^2 + (t-t_c)}]^{0.5} \quad (16)$$

In addition, for high-strength concrete, CEB MC90 model has been developed (CEB 1999) to take into account the particular characteristics of concrete strength. The modified CEB-MC90/99 model subdivides the total shrinkage into the components of drying and autogenous shrinkage (Eq. (17)). Therefore, in the parametric study, this model was used to predict concrete shrinkage for different concrete strength.

$$\varepsilon_{sh(t,tc)} = \varepsilon_{caso(fcm28)} \beta_{as(t)} + \varepsilon_{cdso(fcm28)} \beta_{RH(h)} \beta_{ds(t)} \quad (17)$$

where: f_{cm28} represents concrete mean compressive strength $f_{cm28(ACI318\text{-}11a)} = 1.1 f'_c + 5)$ (MPa), f'_c is the concrete compressive strength (MPa), $\varepsilon_{casa(fcm28)}$ is the nominal autogenous shrinkage coefficient, and $\beta_{as(t)}$ is the function describing the time development of autogenous shrinkage, $\varepsilon_{cdso(fcm28)}$ is the nominal drying shrinkage coefficient, $\beta_{RH(h)}$ is the ambient relative humidity for drying shrinkage, and $\beta_{ds(t)}$ is the function describing the time development of drying shrinkage. It should be noted that, the software takes the concrete creep into account in the materials model. The time-dependent CEB-MC90/99 creep model is implemented in the concrete element for each lead-step increment (day).

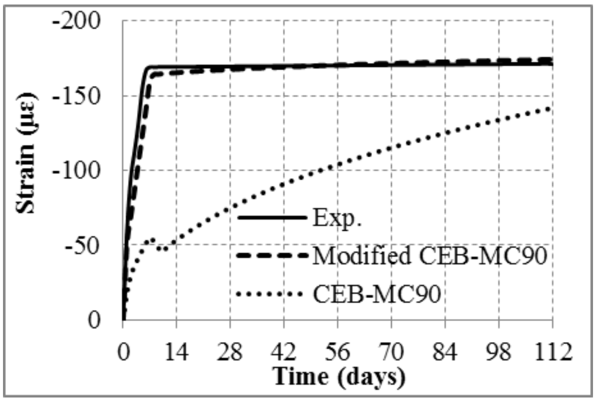

Fig. 6 Experimental and predicted shrinkage values

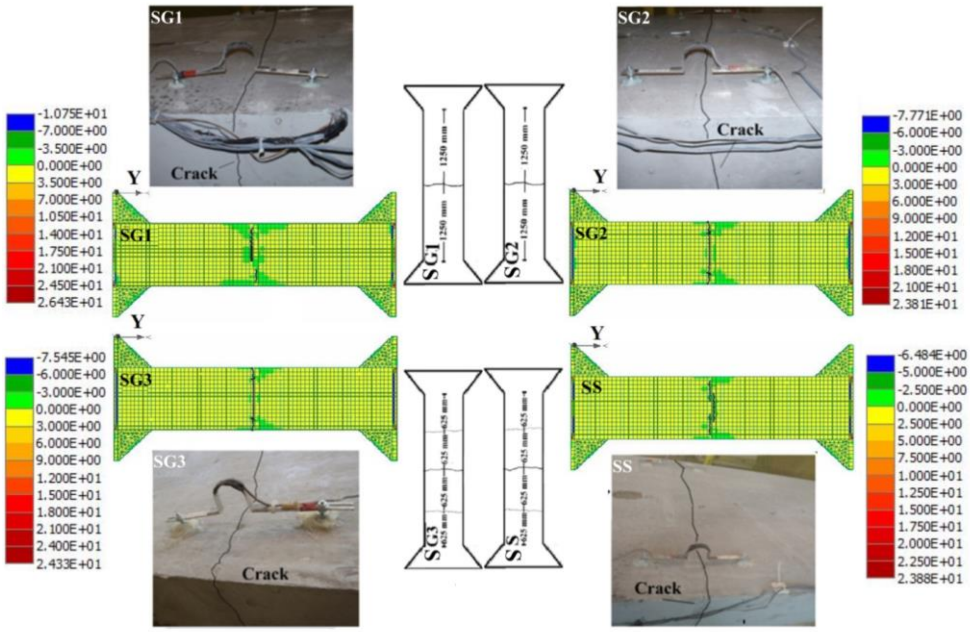

Fig. 7 Concrete stresses in the Y direction (MPa) and cracking pattern

4.6 Analysis

The geometric and material non-linear solution was taken into account by the program using the concept of incremental step-by-step analysis. The shrinkage was applied in 112 load increments; each represents one day of the shrinkage load. At each increment, load iterations were performed until the convergence criteria were satisfied. Four solution errors serve to check convergence criteria: displacement increment normalized residual force, absolute residual force, and energy dissipated (Cervenka *et al.* 2012).

After reaching the equilibrium and completion of each loading step, the stiffness matrix was adjusted to reflect the non-linear changes before proceeding to the next load step. In this regard, the program adopts full Newton-Raphson method to modify the solution parameter. It should be noted that the solving time for running each model was approximately 50 hours.

4.7 Model validation

For the validation process, the experimental results of the four bridge deck slabs were used. The constructed model was calibrated against specimen SG1 and then tested on the remaining specimens to ensure that the results remained within a reasonable error. The model was validated in terms of crack width, crack pattern and average tensile strains in the reinforcement at the crack location. For generalization of the FEM, the predicted shrinkage by modified CEB-MC90 method, assuming wet curing conditions, was also applied to the model. The FEM results for crack width and reinforcement strain remained within a reasonable error of 6% and 10%, respectively. Also, the main crack pattern in the FEM was recorded at a similar location to the experimental program; however, the secondary cracks did not occur in the FEM which were contradicted with the experimental study for specimens SG3 and SS.

Figure 7 shows the cracking pattern for the FEM models and experimental tested slabs. In the experimental study, there was one main crack located at the middle reduced cross section of the slab. The main cracking pattern for the FEM models accurately predicted the crack pattern observed in the experimental program at the middle section. The experimental results indicate that an increase in the reinforcement area or modulus of elasticity (SG3 and SS compared to SG1 and SG2) leads to less stiffness reduction at first cracking (mid-span), thus the restraining force after cracking remains high. With such high restraining force, the development of additional drying shrinkage or temperature variation causes the concrete in regions away from the first crack to experience further cracking. However, the FE results did not record secondary crack pattern on the models for SG3 and SS.

In the FEM, the crack width was considered as the average of the displacements measured by monitoring points at two locations across the slab width at mid-span (replicating the same approach as that of the PI gauges used in the experimental study). Figure 8 represents the crack width development curves for the experimental and the numerical study. The crack width-time diagrams show several important relationships for the models. In the finite element model for SG1 (ρ = 0.5%), the crack width reached the allowable value of 0.5 mm (ACI Committee 440 2015, CSA 2006) after 5 days. After 112 days, this crack width reached 0.67 mm. The FEM results reveal that for SG2 (ρ = 0.7%), SG3 (ρ = 1.1%) and SS (ρ = 0.7%), the crack width were 0.34, 0.26 and 0.20 mm after 112 days. The predicted crack widths in the FEM lie within an average error of 6%. The comparison between the results shows that the FEM was able to accurately predict the final crack width for the GFRP and steel RC slabs (Fig. 8).

In the experimental study, the strains in main reinforcement were measured by strain gauges attached to each rebar at mid-span. A similar approach was followed in the FEM by defining four monitoring points at the same locations. Figure 9 shows the predicted and experimental tensile strains in reinforcement at the cracking location. The results show that, once a crack developed at mid-span, the average strain in reinforcement increased rapidly. This value decreased with increasing the reinforcement ratio or modulus of elasticity. In FEM for SG1, SG2, SG3 and SS, the average strains in the bars at crack location were 2590, 1400, 1130 and 480 $\mu\varepsilon$ after 112 days. However, the strain away from cracking location was still less than 200 $\mu\varepsilon$. The strain in the reinforcement at the crack location was also efficiently predicted by FEM subjected to shrinkage within an average error of 10%.

5. Parametric study

This study examined the effect of concrete compressive strength, concrete cover, reinforcement type, and bar spacing on the early-age behavior of FRP-RC bridge deck slabs subjected to shrinkage. Since the FEM results for SG2 were the closest to those of the experimental results, the parametric study models were developed based on the same assumptions and geometry that were used for modeling slab SG2 in the verification stage. Moreover, the reinforcement ratio for this slab (0.7%) is recommended as the minimum reinforcement ratio for GFRP-RC bridge deck slabs by CHBDC (2006). Table 4 provides details of the parametric FEM. The results are presented in terms of cracking pattern and crack width development and reinforcement strain.

5.1 Concrete compressive strength

In this study, six concrete compressive strengths 30, 40, 50, 60, 70 and 80 MPa were used in the FEM. The applied concrete shrinkage load scheme was obtained according to the CEB MC90-99 method, meeting the requirements of a 3-day moist curing conditions (ACI Committee 209 2008).

The predicted shrinkage values indicate that increasing the strength from 30 to 80 MPa intensifies the autogenous shrinkage and consequently increases the concrete total shrinkage value from 170 to 230 $\mu\varepsilon$ (Table 5). Figure 10(a) shows the typical cracking pattern for different concrete strengths at the notched mid-span location, while Fig. 10(b) illustrates the change in crack width and reinforcement strain over 112 days. As concrete strength was increased from 30 MPa to 80 MPa, the crack width and associated reinforcement strain at crack location grew from 0.33 to 0.48 mm and from 1400 to 2020 $\mu\varepsilon$, respectively. It is well-documented (Mehta and Montherio 2014, Lozano-Galant *et al.* 2014) that, in high-strength concrete (with low water-to-binder ratio), consuming water content during the hydration process intensifies autogenous shrinkage in comparison to normal strength concrete.

This self-desiccation effect was considered in the predicted load scheme by CEB-MC 90/99, as shown in Table 5. Furthermore, bridge deck slabs with high strength concrete offer greater sectional stiffness, which increased the internal restraint, and thus led to an increase in restrained force.

5.2 Concrete compressive strength

In this study, the effect of reinforcement bar spacing on crack control was investigated. A constant reinforcement ratio of $\rho = 0.70\%$ was distributed to 2, 3, 4, 5, 6 and 7 bars (top and bottom) which dictates the spacing ranged between 96 and 255 mm. Figure 11(a) shows the typical cracking pattern for the FEM with different bar spacing at the notched mid-span location. In these models, the cracks typically occurred at mid-span. Results show that reducing the bar spacing from 255 to 96 mm decreases the early-age crack width from 0.34 to 0.29 mm and increases the average value of reinforcement strain from 1400 to 1880 $\mu\varepsilon$, respectively (Fig. 11(b)). These results are in good agreement with previous findings (Frosch *et al.* 2006) which indicate reducing the bar spacing increases the contribution of the reinforcement on early-age crack-width control in bridge deck slabs subjected to shrinkage.

5.3 Concrete cover

The effect of increasing the concrete cover from 5 to 85 mm on crack control was investigated. Figure 12(a) shows the typical crack pattern occurred at mid-span for all models with different thickness of concrete cover. The results in Fig. 12(b) indicate that, for the GFRP-RC members subjected to axial tension (shrinkage) with different concrete covers, the crack width and the average strain on the bar at crack location remain constant within 0.34~0.35 mm and 1320~1330 $\mu\varepsilon$, respectively. The full-depth cracks develop under axial tension (shrinkage) are parallel-sided, which is different from flexural cracks. Therefore, the crack width and strain on the bar at crack location are less dependent on the amount of concrete cover.

5.4 Reinforcement type

Different types of GFRP and Carbon FRP (CFRP) (sand-coated and ribbed-deformed) can be used as internal reinforcement in bridge deck slabs. The magnitude of crack width depends on several factors related to reinforcement type such as quality of bond between concrete and reinforcing bars and modulus of elasticity of reinforcement material (Baena *et al*. 2011). In this study, the effect of reinforcing bar type on crack control was investigated using the constructed FEM with a constant reinforcement ratio of $\rho = 0.70\%$. These models had two different FRP types (CFRP and GFRP) with two different bond characteristics (sand-coated and ribbed-deformed). In addition, since the modulus of elasticity of CFRP bars is higher than that of GFRP, four sand-coated CFRP-RC slabs were simulated with reinforcement ratio of 0.35, 0.40, 0.45 and 0.7%, to obtain the minimum ratio to satisfy code requirements.

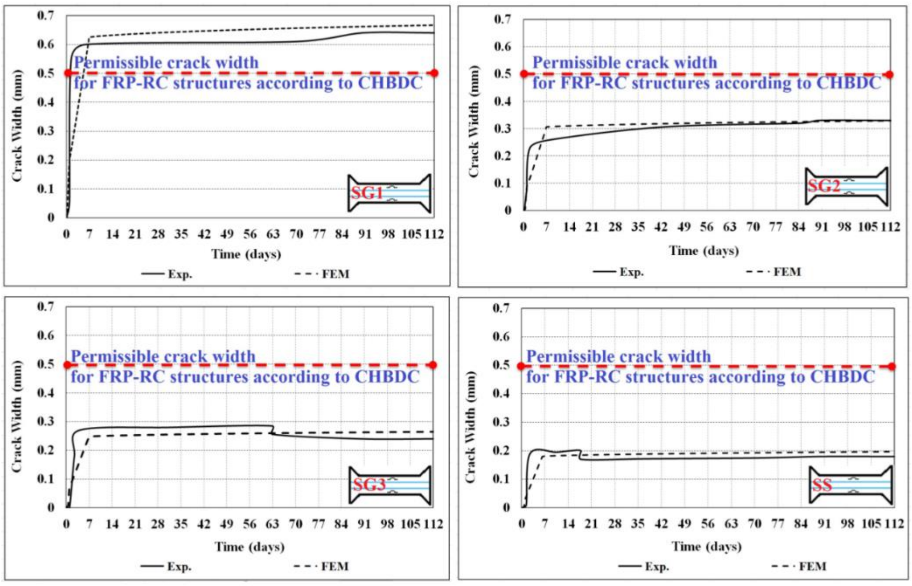

Fig. 8 Experimental and FEM results for the development of crack width with time for slabs SG1, SG2, SG3 and SS

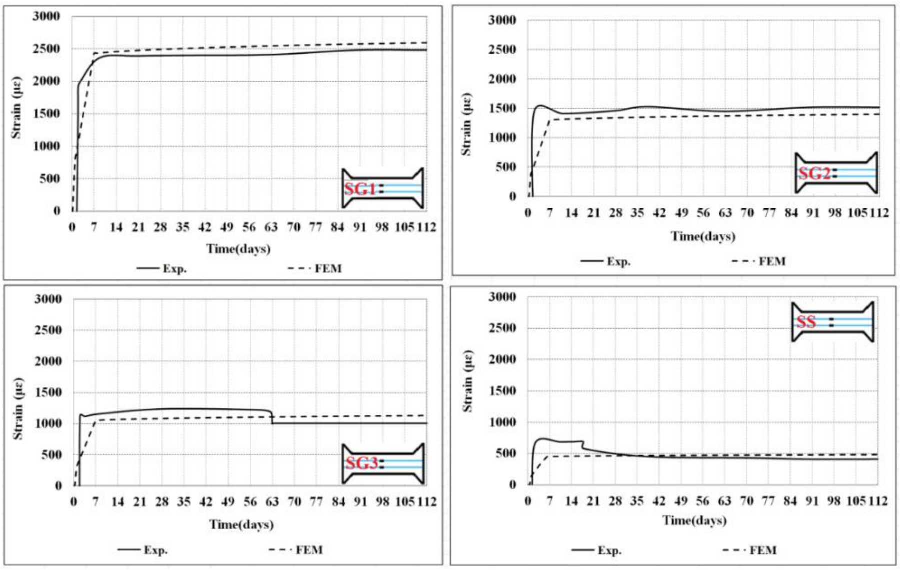

Fig. 9 Experimental and FEM results for the development of bar strains at crack location for slabs SG1, SG2, SG3 and SS

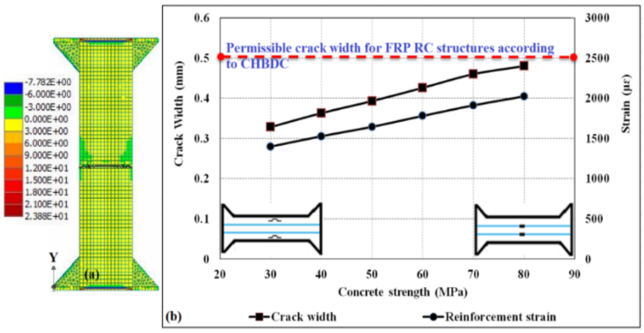

Fig. 10 Results of FEM for slabs with different concrete strength, (a) typical concrete stresses in the Y direction (MPa) and cracking pattern (f_c' = 30 MPa), and (b) development of crack width and average reinforcement strain at cracking with time

Table 4 Test matrix for the FEM

Name	Concrete cover (Bot. & Top) (mm)	Concrete strength (28days) (MPa)	Reinforcement ratio (%)	Bar spacing (mm)	Bar type	Stage
SG1	35&25	38	0.5	255	GFR/Sand coated	Verification
SG2			0.7		GFR/Sand coated	
SG3			1.1		GFR/Sand coated	
SS			0.7		Steel/Ribbed	
G.CS.30	35&25	30	0.7	255	GFR/Sand coated	Parametric study Concrete strength
G.CS.40		40				
G.CS.50		50				
G.CS.60		60				
G.CS.70		70				
G.CS.80		80				
G.CC.5	5&5	38	0.7	255	GFR/Sand coated	Parametric study: Concrete cover
G.CC.15	15&15					
G.CC.25	25&25					
G.CC.35	35&35					
G.CC.45	45&45					
G.CC.55	55&55					
G.CC.56	65&65					
G.CC.75	75&75					
G.CC.85	85&85					
G.BS.96	35&25	38	0.7	96	GFR/Sand coated	Parametric study: Bar spacing
G.BS.127				128		
G.BS.153				153		
G.BS.191				191		
C.SC.0.70	35&25	38	0.70	255	CFR/Sand coated	Parametric study: bond type
C.RB.0.70			0.70		CFR/Ribbed bar	
C.SC.0.70			0.70		GFR/Ribbed bar	
G.RB.0.35	35&25	38	0.35	255	CFR/Sand coated	Parametric study: CFRP bar
G.RB.0.40			0.40		CFR/Sand coated	
G.RB.0.45			0.45		CFR/Sand coated	

[*] Total longitudinal reinforcement ratio, equally, in two layers (top and bottom)

Table 5 The predicted shrinkage value for different concrete strength according to the CEB-MC-90/99 model

Concrete strength (MPa)	Autogenous Shrinkage (με)	Drying Shrinkage (με)	Total Shrinkage (με)
30	58	112	170
40	81	100	181
50	104	88	192
60	127	79	206
70	148	70	218
80	168	62	230

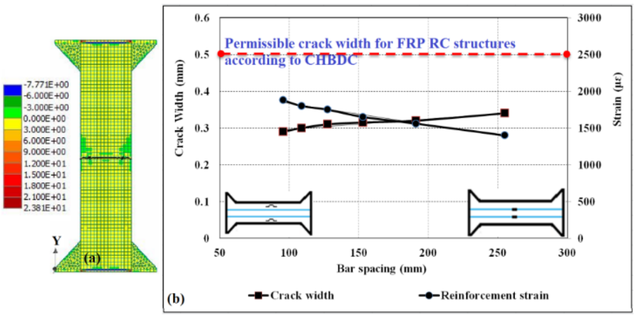

Fig. 11 Results of FEM for slabs with different bar spacing: (a) typical concrete stresses in the Y direction (MPa) and cracking pattern (for spacing: 255 mm), and (b) development of crack width and average reinforcement strain at cracking with time

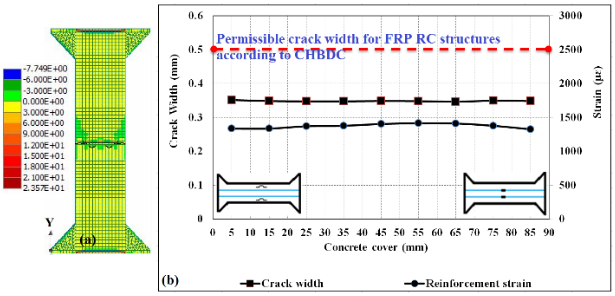

Fig. 12 Results of FEM for slabs with different concrete cover: (a) typical concrete stresses in the Y direction (MPa) and cracking pattern (for cover: 5 mm), and (b) development of crack width and average reinforcement strain at cracking with time

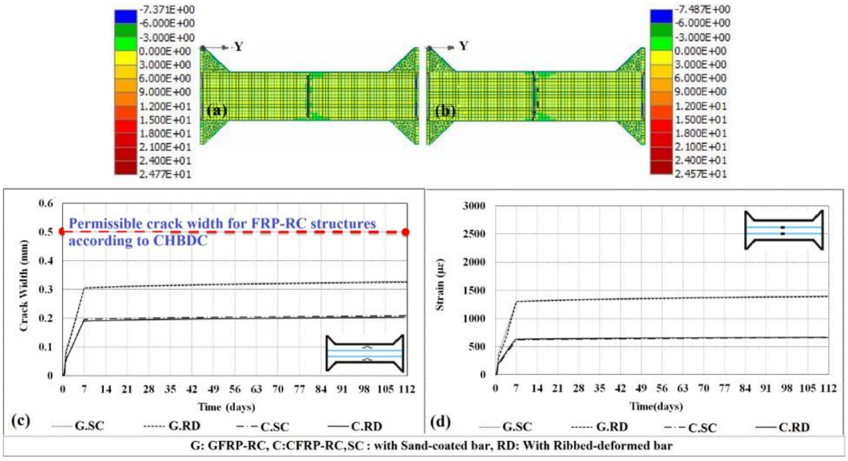

Fig. 13 Results of FEM for slabs with different bar type: (a) typical concrete stresses in the Y direction (MPa) and cracking pattern for GFRP, (b) typical concrete stresses in the Y direction (MPa) and cracking pattern for CFRP, (c) development of crack width with time, and (d) development of the bar strains at crack location for the FEM

Figures 13(a) and 13(b) shows typical cracking pattern for FEM at the notched mid-span location. Using a reinforcement ratio of 0.70% sand-coated CFRP bars resulted in a final crack width and average bar strain of 0.21 mm and 660 με, respectively (Figs. 13 (c) and 13(d)). These values were 0.33 mm and 1400 με, respectively, for thecounterpart slab with GFRP bars. This was expected due to lower modulus of elasticity GFRP bars compared to that of CFRP. Nevertheless, the results for crack width and average strain on the bars at crack location (Figs. 13 (c) and 13(d)) show that the change in bond slippage characteristics (sand-coated to ribbed-deformed bar) has insignificant effect on the results. This may be attributed to the similar bond stress-slippage behavior for sand-coated and ribbed bars (GFRP and CFRP) at low induced stress surrounding the reinforcement in the vicinity of the crack (Alves *et al.* 2011).

The stress surrounding the reinforcement at crack location calculated by Gilbert's equation (Gilbert 1992) for sand-coated and ribbed-deformed CFRP bars were 0.73 and

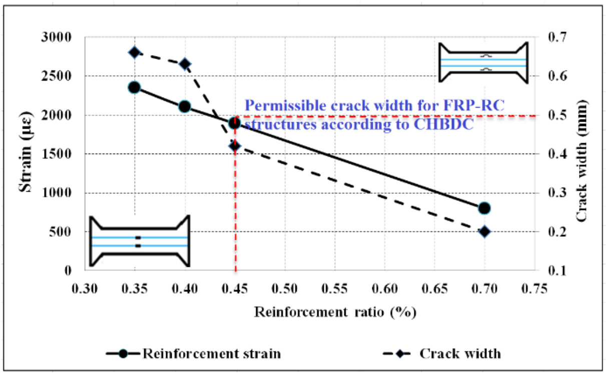

Fig. 14 The crack width and average reinforcement strain (Top and Bot.) at cracking location for the FE models reinforced with CFRP bars at 112 days

0.74 MPa, respectively. However, this value for sand-coated and ribbed-deformed GFRP bars was 0.62 and 0.63 MPa, respectively. Test results indicate that primarily width of the crack in the models reinforced with CFRP bars varied depending on the reinforcement ratio crossing the crack.

Figure 14 shows that increasing the reinforcement ratio from 0.35 to 0.7 %, decreased crack width and reinforcement strain at crack location from 0.66 to 0.21 mm and from 2350 to 660 με, respectively. Also, test results indicate that a ratio of 0.45% can control the early-age crack width and reinforcement strain in CFRP-RC bridge deck slabs subjected to shrinkage. In the model reinforced with 0.45% CFRP bars, the maximum crack width and CFRP strain were 0.42 mm and 1890 με, respectively. These values are below the allowable code limit of 0.5 mm and 7650 με (65% of CFRP ultimate strain), respectively (CHBDC 2006).

6. Conclusions

This study aimed at investigating the effect of four key variables including concrete cover, concrete strength, reinforcement type, and bar spacing on the early-age behavior of FRP-RC bridge deck slabs subjected to restrained shrinkage through a finite element analysis. The primary findings of this study can be summarized as follows:

- The constructed FEM was able to analyze FRP-RC bridge deck slabs subjected to restrained shrinkage. The FEM could predict the maximum crack width and the main cracking pattern as well as the strains developed in the reinforcement at the vicinity of the crack to a reasonable degree of accuracy (within 6 to 10% for crack width and reinforcement strain at the crack location, respectively).
- The results indicate that increasing concrete strength in RC bridge deck slabs increases the early-age crack width. At 112 days, as concrete strength increased from 30 to 80 MPa, the crack width and reinforcement strain at crack location grew from 0.33 to 0.48 mm and from 1400 to 2020 με, respectively. This is attributed to the higher autogenous shrinkage and induced tensile stresses in the slabs.
- In RC bridge deck slabs subjected to restrained shrinkage, reducing the bar spacing results in decreasing the crack width and increasing the reinforcement strain at crack location. In the FEM with constant reinforcement ratio of 0.7%, decreasing bar spacing from 255 to 96 mm reduced the crack width from 0.34 to 0.29 mm and increased the average value of reinforcement strain from 1400 to 1880 με. .
- Results from the parametric study indicate that for the FRP-RC members subjected to axial tension (shrinkage), the crack-width and strain in the bars at crack location are less dependent on the thickness of concrete cover. This is due to the fact that shrinkage cracks are full-depth and parallel-sided.
- Due to the relatively lower modulus of elasticity of GFRP bars, the crack width and average reinforcement strain in the GFRP RC slab were 1.6 and 1.1 times, respectively larger than those of the corresponding slab reinforced with similar CFRP reinforcement ratio of 0.7%. Nevertheless, the results for crack width and average strain in the bars at crack location show that the change in bond slippage characteristics (sand-coated to ribbed-deformed bar) has insignificant effect on the results.
- A reinforcement ratio of 0.45% can keep the early-age crack-width and reinforcement strain within the allowable code limits (CHBDC 2006) of 0.5 mm and 7650 με (65% of CFRP ultimate strain), respectively.

Acknowledgments

The financial support provided by the Natural Science and Engineering Research Council of Canada (NSERC) through Canada Research Chairs (CRC) program and the Centre for Structural Innovation and Monitoring Technologies Inc (SIMTReC) are gratefully appreciated. Also, the assistance of K. Speidel (MMM/WSP) and the technical staff of the McQuade Heavy Structures Laboratory at the University of Manitoba are greatly appreciated.

References

ACI Committee 209 (2008), *Guide for Modeling and Calculating Shrinkage and Creep in Hardened Concrete*, ACI 209.2R-08, American Concrete Institute, Farmington Hills, Michigan, U.S.A.

ACI Committee 440 (2003), *Guide for the Design and Construction of Concrete Reinforced with FRP Bars*, ACI 440.IR-03, American Concrete Institute, Farmington Hills, Michigan, U.S.A.

ACI Committee 440 (2015), *Guide for the Design and Construction of Structural Concrete Reinforced with FRP Bars*, ACI 440.IR-15, American Concrete Institute, Farmington Hills, Michigan, U.S.A.

Alves, J., El-Ragaby, A. and El-Salakawy, E. (2011), “Durability of GFRP bars bond to concrete under different loading and environmental conditions”, *J. Compos. Constr.*, **15**(3), 249-262.

ASTM Standards (ASTM E-831) (2013), “Standard test method for linear thermal expansion of solid materials by thermomechanical analysis", ASTM International (ASTM E831-13), U.S.A.

Au, F.T.K., Liu, C.H. and Lee, P.K.K. (2007), "Shrinkage analysis of reinforced concrete floors using shrinkage-adjusted elasticity modulus", *Comput. Concrete*, **4**(6), 437-456.

Baena, M., Turon, A., Torres, L. and Mias, C. (2011), "Experimental study and code predictions of fibre reinforced polymer reinforced concrete (FRP-RC) tensile members", *Compos. Struct*., **93**, 2511-2527.

Canadian Standards Associations (CSA) (2006), *Canadian Highway Bridge Design Code-CHBDC*, CAN/CSA-S6-06, Toronto, Canada.

Canadian Standards Associations (CSA) (2012), *Design and Construction of Building Structures with Fibre-Reinforced Polymers*, A National Standard of Canada (CSA/S806-12), Canadian Standards Association, Toronto, Canada.

CEB-FIP (1990), *Model Code for Concrete Structures*, Comite Europeen du beton, Paris, France.

CEB (1999), *Structural Concrete: Behaviour, Design and Performance*, Updated Knowledge of the CEB-FIP Model Code 1990, fib Bulletin 2, Federation International du Beton, Lausanne, Switzerland, 37-52.

Cervenka, V. and Niewald, J. (2005), *ATENA-FEMAP User's Guide*, Cervenka Consulting Ltd., Prague, Czech Republic.

Cervenka, V., Jendele, L. and Cervenka, J. (2012), *ATENA Program Documentation, Part 1: Theory*, Cervenka Consulting Ltd., Prague, Czech Republic.

Chen, H.J., Liu, T. and Tang, C. (2008), "Numerical modeling of drying shrinkage behavior of self-compacting concrete", *Comput. Concrete*, **5**(5), 435-448.

Frosch, R., Brice, J. and Ericson, J. (2006), *Design Methods for the Control of Restrained Shrinkage Cracking*, Final Report, Joint Transportation Research Program, Project no. C-36-56MMM, File No. 7, 4-63.

Ghatefar, A., El-Salakawy, E. and Bassuoni, M. (2014), "Effect of reinforcement ratio on transverse early-age cracking of GFRP-RC bridge deck slabs", *J. Compos. Constr*., **18**(6), 04014018.

Gilbert, R.I. (1992), "Shrinkage cracking in fully restrained concrete members", *ACI Struct. J*., **89**(2), pp. 141-149.

Hadidi, R. and Saadeghvaziri, M.A. (2005), "Transverse cracking of concrete bridge decks: State-of-the-art", *J. Bridge Eng*., **10**(5), 503-510.

ISIS Canada (2007), *Reinforcing Concrete Structures with Fibre Reinforced Polymers*, The Canadian Network for Centers of Excellence on Intelligent Sensing for Innovative Structures (ISIS-M03-07), Winnipeg, MB, Canada.

Koenigsfeld, D. and Myers, J.J. (2003), *Secondary Reinforcement for Fibre Reinforced Polymers Reinforced Concrete Panels*, Center for Infrastructure Engineering Studies (CIES 03-45), University of Missouri, Missouri, Rolla.

Kwan, A.K.H. and Ng, P.L. (2009), "Shrinkage movement analysis of reinforced concrete floors constructed in stages", *Comput. Concrete*, **6**(2), 167-185.

Lozano-Galant, J.A. and Turmo, J. (2014), "Creep and shrinkage effects in service stresses of concrete cable-stayed bridges", *Comput. Concrete*, **13**(4), 483-499.

Malvar, L.J., Cox, J.V. and Cochran, K.B. (2003), "Bond between carbon fiber reinforced polymer bars and concrete. I: Experimental study", *J. Compos. Constr*., **7**(2), 154-163.

Mazaheripour, H., Barros, J.A.O., Sena-Cruz, J.M., Pepe, M. and Martinelli, E. (2013), "Experimental study on bond performance of GFRP bars in self-compacting steel fiber reinforced concrete", *J. Compos. Struct*., **95**, 202-212.

Mehta, P.K. and Montherio, P.J.M. (2014), *Concrete: Microstructure, Properties, and Materials*, McGraw Hill, New York, U.S.A.

Mias, C., Torres, L., Turon, A. and Barris, C. (2013), "Experimental study of immediate and time-dependent deflections of GFRP reinforced concrete beams", *J. Compos. Struct*., **96**, 279-285.

Minnetyan, L. (2011), *Tool for Analysis of Early Age Transvers Cracking of Composite Bridge Decks*, Final report, Joint Transportation Research Program, Project No. SPR-06-37(C-06-37), Clarkson University, New York, U.S.A.

Myers, C. (1982), *Survey of Cracking on Underside of Classes B-1 and B-2 Concrete Bridge Decks in District 4*, Investigation No. 82-2, Division of Material and Research, Missouri Highway and Transportation Department, Jefferson, Missouri, U.S.A.

Ramey, G.E., Wolff, A.R. and Wright, R.L. (1997), "Structural design actions to mitigate bridge deck cracking", *Prac. Period. Struct. Des. Constr*., **2**(3), 118-124.

RILEM Technical Committee (1988), *Material Models for Structural Creep Analysis*, Chapter 2 in Mathematical Modeling of Creep and Shrinkage of Concrete, 99-215, New York, U.S.A.

Sooriyaarachchi, H., Polakoutas, K. and Byars, F. (2005), "Tension stiffening behavior of GFRP-reinforced concrete", *Proceedings of the 7th International Symposium on Fiber-Reinforced Polymer (FRP) Reinforcement for Concrete Structures (FRPRCS-7)*, Kansas, Missouri, U.S.A., November.

Zhang, J., Gao, Y., Han, Y. and Sun, W. (2012), "Shrinkage and interior humidity of concrete under dry-wet cycles", *J. Dry. Technol*., **30**(6), 583-596.

CC